This article has been accepted for publication in IEEE Transactions on Antennas and Propagation. This is the author's version which has not been fully edited and content may change prior to final publication. Citation information: DOI 10.1109/TAP.2022.3188354

High-Contrast Low-Loss Antenna: A Novel Antenna for Efficient Into-Body Radiation

Allyanna Rice, *Student Member, IEEE*, and Asimina Kiourti, *Senior Member, IEEE*

***Abstract*— We present a biocompatible high-contrast low-loss antenna (HCLA) designed for efficient into-body radiation for applications as diverse as medical telemetry, sensing, and imaging. The HCLA is wearable with a compact size of 2.62 cm^3 and operates across the 1 to 5 GHz bandwidth. The quasi-bowtie antenna is loaded with a high-contrast (i.e., alternating layers of high and low permittivity materials) and low-loss dielectric to improve directivity and gain into the biological tissues. Measurement results at 2.4 GHz are in good agreement with simulations and show 5.72 dB improvement in transmission loss over the most efficient into-body radiator reported in the past. At the high end of the frequency bandwidth, simulation results for two antennas placed across each other with tissue in between show ~12.5 dB improvement in transmission loss. The HCLA is fabricated with stable, low-loss materials that allow for repeatability and consistency in the fabrication process, thus, addressing limitations of the current state-of-the-art. It is also made from biocompatible materials that enable it to be placed directly on the skin for real-world implementation. In this paper, we discuss the operation principle and design of the HCLA, its transmission performance, radiation patterns, and specific absorption rate.**

***Index Terms*— Biomedical telemetry, into-body antenna, wearable antenna, engineered dielectric**

I. Introduction

APPLIED electromagnetics (EM) in the form of sensors, wearables, and implants is critical to many medical device technologies. The emergence of wireless implants and the development of non-invasive sensing techniques offer the potential to solve several current and future healthcare problems. For example, the development of wireless implants necessitates efficient wireless communication to external monitoring and control equipment, as well as wireless chargers and power systems [1]–[9]. Medical radiometry involves noninvasive, passive imaging of internal body temperature from natural emissions at radio frequencies [10]–[13]. Microwave tomography offers a new biomedical imaging technique involving measuring variations in biological tissues and has been used to detect cancerous tumors [14], [15]. The aforementioned medical technologies all require efficient, robust, and wearable into-body antennas, i.e., antennas that radiate towards the human body instead of away from it.

The key attributes for an into-body antenna are high gain and, depending on the application, wide bandwidth (e.g., to allow for multi-band telemetry or to sense black body radiation from across different tissue depths [16]). Indeed, the design of into-body antennas has been of interest in several works. Several designs involve placing the antenna away from the body, creating a considerable air gap between the antenna and the tissue [1]–[6]. This setup produces significant mismatch loss at the air-tissue interface due to the high permittivity, lossy tissues. Other designs involve placing the external antenna directly on the tissue for communication with the implant [7]–[9], [17], [18]. Patch antennas are often selected due to their conformality to the skin [7]–[9], but do not have a wide bandwidth or address biocompatibility concerns. In other cases, such as for radiometry applications, antenna designs are concerned with the bandwidth or post-processing data algorithms, rather than transmission loss of the antenna [10]–[13]. Therefore, the antennas are not efficient radiators into the tissue which impacts the accuracy of the received thermal radiation.

With these in mind, we recently demonstrated a class of wearable, into-body antennas that outperform previous designs in both gain and bandwidth [17], [18]. We referred to these antennas as Bio-Matched Antennas (BMAs) since they rely on periodic combinations of plastic and water (or hydrogel) to mimic the frequency-dependent permittivity of biological tissues, and, hence, reduce mismatch loss. However, a major limitation of the design is that water (or hydrogel) has a very high loss tangent ($\tan\delta = 0.157$ at 3 GHz [19]) resulting in power loss of EM fields prior to the fields penetrating the tissue. Another limitation lies in the fabrication process that is prone to errors and exhibits poor repeatability [20]. Specifically, a 3D-printed dielectric lattice must be filled with water or hydrogel which leads to frequent and unpredictable air bubbles and air holes. Consistent fabrication of the antenna is difficult to achieve. Finally, the use of water (or hydrogel) in the antenna makes the antenna unstable [20]. The antenna is only usable in the hours immediately after fabrication before the performance degrades due to changes in the concentration of the dielectric (due to water leakage, hydrogel dryness, evaporation, etc.).

This work was supported by a NASA Space Technology Graduate Research Opportunities Award. Research reported in this work was also supported by the National Institute Of Biomedical Imaging And Bioengineering of the National Institutes of Health under Award Number R03EB030286. The content is solely the responsibility of the authors and does not necessarily represent the official views of the National Institutes of Health.

The authors are with the ElectroScience Laboratory, Department of Electrical and Computer Engineering, The Ohio State University, Columbus, OH 43210 USA (email: rice.1091@osu.edu; kiourti.1@osu.edu)

This article has been accepted for publication in IEEE Transactions on Antennas and Propagation. This is the author's version which has not been fully edited and content may change prior to final publication. Citation information: DOI 10.1109/TAP.2022.3188354

TABLE I
COMPARISON OF INTO-BODY ANTENNAS

	BMA [17], [18]	HCLA (proposed)
Operating Principle	Match dielectric permittivity to frequency-dependent permittivity of tissues	Alterations of high and low permittivity materials with extremely low loss
Materials	Polylactic Acid (ε_r = 3.549 and tanδ = 0.001) and Hydrogel (ε_r = 77 and tanδ = 0.157)	Polylactic Acid (ε_r = 3.549 and tanδ = 0.001) and Zirconia Oxide (ε_r = 29 and tanδ = 0.001)
Repeatable fabrication	No	Yes
Stable operation over time	No (shelf life: < 1 day)	Yes (shelf life: months to years)
Size	22 x 22 x 10 mm^3	25.1 x 25.1 x 12.5 mm^3
10 dB Bandwidth	1.4 – 8.5 GHz	1.38 – 4.95 GHz
Transmission Loss to Implant	27.50 dB at 2.4 GHz	21.78 dB at 2.4 GHz
Balun	Omitted, though required for practical applications	Yes

In this work, we take a major step forward and demonstrate that "bio-matching" the antenna's dielectric to tissues is actually not as important as is the alteration of high- and low-permittivity materials with extremely low loss. We, thus, advance the concept of BMAs to High-Contrast Low-Loss Antennas (HCLAs) instead. The idea is to design the dielectric in a way that forces the EM waves to propagate towards tissue in a directed manner while eliminating loss on the material itself. As a proof-of-concept, zirconia oxide (ε_r = 29 and tanδ = 0.001 [21]) and polylactic acid (ε_r = 3.549 and tanδ = 0.001 [22]) are selected as materials for the dielectric. Compared to the BMA, the HCLA is shown to reduce loss by ~5.72 dB at 2.4 GHz (an Industrial, Scientific, Medical, ISM, frequency) and ~12.49 dB at 4.8 GHz (a frequency used for implants in [23], [24] and for radiometry in [16]). Though these materials are not limiting, their biocompatibility allows for direct placement on the skin. Additional advantages of HCLAs as compared to BMAs entail: (a) reproducibility of the fabrication approach, and (b) stability over time, as will be demonstrated in this work. Last but not least, this is the first time that a balun is incorporated in our quasi-bowtie into-body antennas, hence further improving the EM performance stability as compared to our previously reported BMAs. A comparison of BMAs vs. HCLAs is shown in Table I. It is important to note that the bandwidth of the HCLA is smaller, with a high frequency cutoff of 4.95 GHz rather than 8.5 GHz; however, frequencies above 5 GHz do not radiate efficiently into the tissue and are typically disregarded in most biomedical applications [25].

The rest of this paper is organized as follows. Section II discusses the operation principle of the high-contrast low-loss antenna. Section III presents the antenna design and simulation setup. Section IV describes the antenna fabrication and experimental setups. Section V discusses the performance of the HCLA. The paper concludes in Section VI.

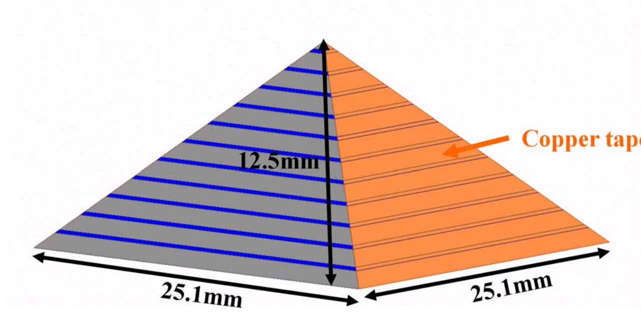

Fig. 1. Proposed pyramidal HCLA with a dielectric made from layers of Zirconia Oxide (gray) and Polylactic Acid (blue).

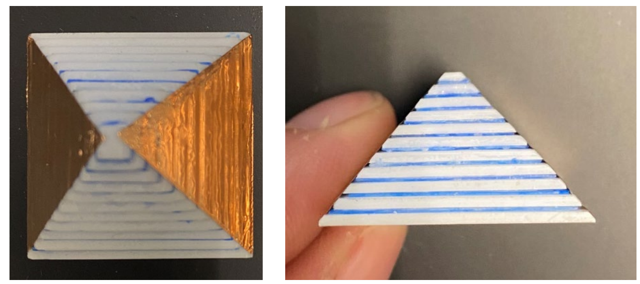
(a) (b)
Fig. 2. (a) Side view of the antenna dielectric with layers of ceramic (white) and plastic (blue) and (b) Top view of the antenna dielectric and copper tape conductors.

II. OPERATION PRINCIPLE

The HCLA is shown in Fig. 1 and is best described as a quasi-bowtie antenna [26] due to the shape of the conductors and the feeding mechanism. Its top-down view, Fig. 2(a), visually looks exactly like a traditional bowtie antenna, as known to empower wide bandwidth. Additionally, the frequency of operation for the HCLA is dependent on the length and width of the bowtie flares. However, the conductors do not lie in the same plane and are approximately perpendicular to each other, hence the term quasi-bowtie, Fig. 2(b). The 3D pyramidal shape of the substrate resembles the structure of a horn antenna. Horn antennas are beneficial as into-body radiators because of their high gain and broadband operation. As such, the antenna also demonstrates similar behavior to a horn antenna that is loaded, in our case, with a dielectric material. In particular, loading a horn antenna with an engineered dielectric has been proven to improve the gain and directivity of the antenna [27]–[30]. A metamaterial lens placed inside the horn transforms outgoing spherical waves into planar wavefronts with more directive emission. The lens also narrows the primary lobe and increases its intensity while suppressing the side lobes, further improving directivity. It is important to note that in [27]–[30], the entirety of horn is not loaded, but rather a lens is placed near the opening of the horn. The lens is successful in a traditional horn where all four sides of the horn are conductors. The HCLA, however, only has conductors on two sides of the pyramidal shape with horn-like characteristics. If a lens is used rather than fully loading the dielectric, EM waves will escape from the sides where conductors are not present. With the above in mind, the

This article has been accepted for publication in IEEE Transactions on Antennas and Propagation. This is the author's version which has not been fully edited and content may change prior to final publication. Citation information: DOI 10.1109/TAP.2022.3188354

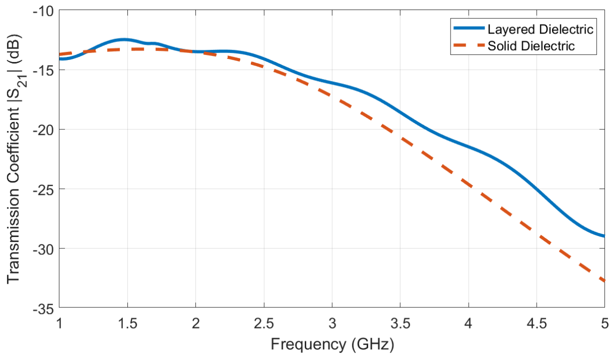

Fig. 3. Simulated transmission coefficient of the HCLA with a layered dielectric versus a solid dielectric

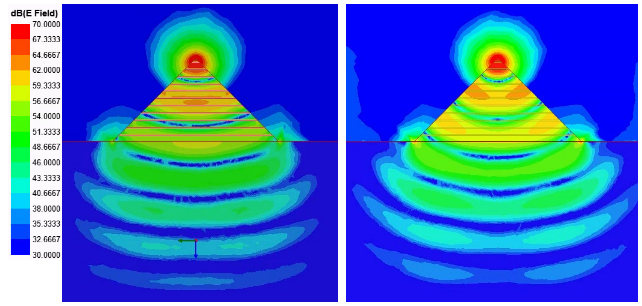

(a) (b)

Fig. 4. Simulated electric field patterns of the HCLA at 5 GHz with a (a) layered dielectric and (b) solid dielectric

HCLA entails a fully loaded dielectric to better contain the waves than the air. It is also important to note that placing conductors on all four sides of the pyramid (like a traditional horn antenna) was considered, but not pursued because the frequency of a horn antenna is based on the aperture size. The aperture for 1 to 5 GHz would have to be quite large and is thus inappropriate for wearable applications.

Designing antennas that radiate efficiently into the body is a significant challenge due to the lossy properties of the human tissue. A very low or very high permittivity material will create a significant mismatch at the antenna-skin interface. Selecting the material with the best impedance match is important to minimize reflection losses and improve transmission. We could have designed the antenna with a single solid dielectric material; however, we knew that given the pyramidal shape of the dielectric, lensing could further improve gain and directivity. We design a metamaterial dielectric consisting of alternating layers of high and low permittivity materials with a periodic structure at the sub-wavelength scale in the 1 to 5 GHz range to produce both matching and lensing effects.

By contrast to BMAs, our goal is not to perfectly match the permittivity and loss tangent of tissues to that of the antenna's dielectric, but rather to minimize mismatch and enhance contrast in the dielectric stack in a way that sends the fields towards the human body in a directive manner. This is achieved by engineering higher permittivity paths in the direction parallel to the tissue surface (unwanted direction) as compared to the direction towards the tissue (wanted direction). Simulations verified that alternating high and low permittivity materials significantly improved transmission across the bandwidth compared to a dielectric composed of a single high permittivity material, as seen in Fig 3. Simulations of the electric field also verified the alternating layers produce a more planar wavefront (Fig. 4(a)) than the solid dielectric (Fig. 4(b)). As seen in Fig. 4(a), the wavefronts look spherical inside of the horn antenna but become planar as they leave the engineered dielectric and enter the biological tissues, particularly in the tissue that is directly below the antenna. These planar wavefronts improve directivity and gain. Also, key to our approach is materials that are low loss to reduce the transmission loss across the bandwidth. By contrast, BMAs utilized high-loss water/hydrogel to match the properties of biological tissues which compromised their transmission performance.

III. Antenna Design and Simulation Setup

The proposed HCLA is illustrated in Fig. 1. The antenna is compact with a small volume of 2.62 cm^3 so that it will fit comfortably on the body with no airgap between the antenna and the skin. The HCLA is smaller or comparable to other into-body antennas in the literature ([6], [8]–[13], [16]–[18]). It is designed to operate in the 1 to 5 GHz frequency range that includes, among others, the 1.4 GHz Wireless Medical Telemetry Services (WTSM) band and the 2.4 GHz Industrial, Scientific, Medical (ISM) band. This frequency range has also been used repeatedly for radiating into the tissue [16], [25]. The primary optimization criteria are that: (a) the reflection coefficient, $|S_{11}|$, should be below -10 dB across the bandwidth, and (b) the transmission coefficient, $|S_{21}|$, should be as high as possible to minimize the transmission loss in the tissues between two antennas. Additional criteria include antenna size; feasibility of fabrication; and biocompatibility. In our case, the low frequency cutoff is determined by the size of the antenna. Increasing the size of the antenna will lower the low cutoff frequency. It is important, however, to consider the tradeoff between increasing the size of the antenna and the wearability. The high frequency cutoff was not analyzed due to the small penetration depth of EM waves into biological tissues at higher frequencies [25].

The design and optimization of the HCLA was performed using finite element simulations in Ansys High Frequency Simulation Software. The antenna was placed upon a 7.5 cm by 7.5 cm tissue-emulating box (2/3 muscle with frequency-dependent dielectric properties [31]) with a thickness of 3 cm, Fig. 5(a). The first step was to determine the ideal permittivity for the high permittivity material in the dielectric. The HCLA loaded with a solid dielectric material (i.e., no low permittivity layers) was analyzed. Parametric studies were performed for a material with relative permittivities between 5 to 80 and a low loss tangent of 0.001. Larger dielectric losses were found to degrade performance. Lower permittivities were found to have a higher transmission coefficient at higher frequencies and higher permittivities were found to have a higher transmission coefficient at lower frequencies. Because the tissues are frequency-dependent, the relative permittivity of the tissues is higher at lower frequencies and lower at higher frequencies. Thus, it makes sense that higher permittivity materials would match better at lower frequencies, and lower permittivity materials would match better at higher frequency materials. To

This article has been accepted for publication in IEEE Transactions on Antennas and Propagation. This is the author's version which has not been fully edited and content may change prior to final publication. Citation information: DOI 10.1109/TAP.2022.3188354

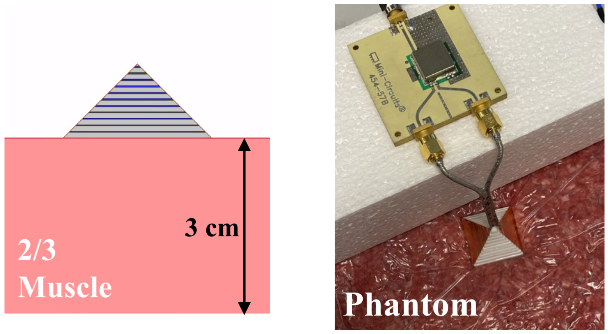

(a) (b)

Fig. 5. (a) Simulation setup and (b) experimental setup in this study.

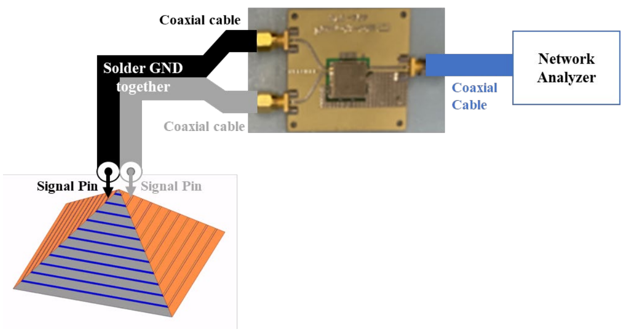

Fig. 6. Experimental feeding mechanism for the HCLA

design a broadband antenna, we need to compromise and select a permittivity that is efficient across the entire frequency range, which in this case is between 25 and 35. This range has the highest average transmission coefficient across the entire bandwidth, while also maintaining a reflection coefficient below -10dB. This range of permittivities is lower than the dielectric constant of skin (ε_r = 38.06 at 2.4 GHz [31]) proving a perfect match is not necessary as claimed in [18].

Zirconia Oxide, an oxide ceramic, is selected as the high-permittivity low-loss material (ε_r = 29 and tanδ = 0.001, Table I). Zirconia is often described as "ceramic steel" due to its mechanical strength and toughness, and is a biomaterial that is commonly used in surgical and dental implants due to its desirable properties [33]. It is commercially available in several forms including rods, substrates, and plates.

Next, a low permittivity material must be layered between the high permittivity material to engineer the subwavelength metamaterial dielectric, thus, improving gain and directivity per discussion in Section II. The low permittivity material for the dielectric was selected to be polylactic acid (PLA) filament (ε_r = 3.549 and tanδ = 0.001, Table I). PLA is also a biocompatible material and is used for many different applications including tissue engineering, resorbable sutures, dental materials, and drug delivery systems [34]. PLA is easily fabricated into any shape and size with current high-resolution 3D printing technology.

In summary, besides their desired electrical properties, the high and low permittivity materials for the HCLA dielectric are also selected for their biocompatibility (to allow the antenna to be safely placed directly on the skin, as regulated by the U.S. Food and Drug Administration [35]) as well as ease, stability, and repeatability of fabrication. The properties of the materials will not change over time, as was problematic in [20], and both are mechanically and thermally stable. The antenna, once

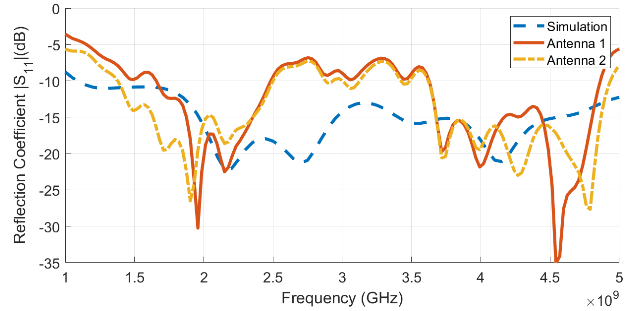

Fig. 7. Simulated versus measured reflection coefficient ($|S_{11}|$) of two identically fabricated antennas.

fabricated, will have the same performance several weeks, months, or even years later. Of course, different high or low permittivity materials could be selected if different relative permittivity or loss tangent values are required, but fabrication may need to be reconsidered.

After determining the materials, the ideal ratio of the high permittivity (Zirconia) to low permittivity (PLA) within the dielectric was determined. The Zirconia is available from the manufacturer in a fixed thickness of 0.914 mm [36]. The PLA can vary in thickness, limited only by the minimum resolution of the 3D printer. To determine the optimal ratio of Zirconia to PLA, a parametric study was performed. The optimal thickness for the PLA was determined to be 0.185 mm, creating single layer of combined ceramic and plastic that is 1.1 mm. This ratio resulted in the lowest cutoff frequency without a compromise in size.

Lastly, the quasi-bowtie HCLA is balanced and needs a balun for connecting to an unbalanced coaxial cable. Due to the broadband performance of the antenna, a commercial off-the-shelf transformer balun was selected and incorporated in simulations, Mini-Circuits part SCTX1-83-2W+ [37]. This balun is mounted on a large evaluation board from the manufacturer for ease of fabrication and testing. A smaller balun that is more appropriate for wearable applications could be designed but is beyond the scope of this study.

IV. Antenna Fabrication and Experimental Setup

The HCLA was fabricated by stacking layers of Zirconia and PLA. The ceramic substrate was ordered from Ortech Ceramics and came in 114.3 mm^2 squares with a thickness of 0.9144 mm [36]. The substrate was diced with a diamond blade into squares varying in size from 25.1 mm^2 to 0.9 mm^2 to create the pyramidal layers as seen in Fig. 2(b). The PLA layers of varying square sizes were printed using rigid resin [38] with a Formlabs Form2 3D printer [39]. The alternating layers of Zirconia and PLA were stacked from largest to smallest. Super glue was used in between each layer to form the pyramidal structure. A rotary tool was used to grind the sides of the pyramid into the smooth 45° angles as seen in Fig. 2(b). Copper tape was cut into triangles and placed on two sides of the pyramid to serve as the conductors of the antenna, similar to how copper could be etched on a planar substrate. The balun was soldered directly to the copper tape conductors. The complete feeding mechanism for the antenna is illustrated in Fig. 6. Notably, this fabrication process is not prone to the many errors of our previous work described in [20]: the materials are manufactured to exact sizes,

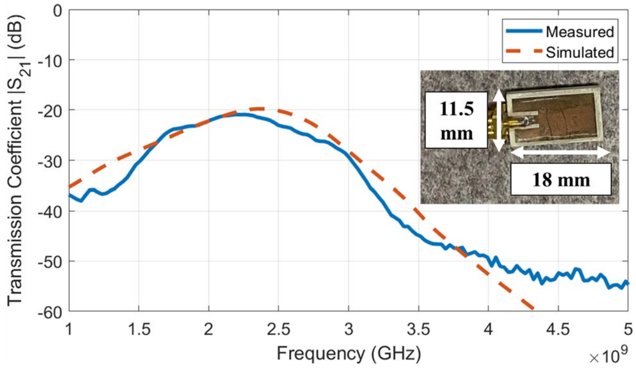

Fig. 8. Simulated versus measured transmission coefficient (|S_{21}|) between the HCLA and the 2.4 GHz implanted patch antenna.

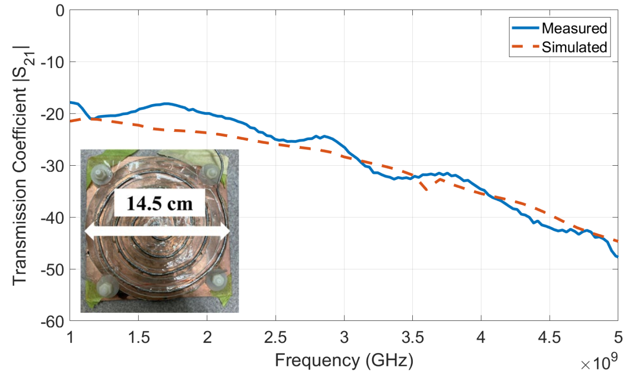

Fig. 9. Simulated versus measured transmission coefficient (|S_{21}|) between the HCLA and the broadband spiral antenna.

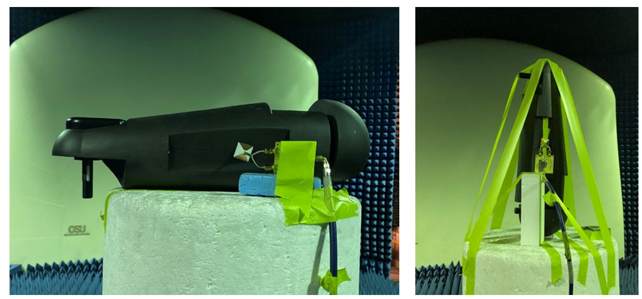

(a) (b)

Fig. 10. Measurement setup with the antenna, balun, and POPEYE phantom in the anechoic chamber at The Ohio State University (a) in the horizontal orientation and (b) in the vertical orientation.

the layers are easily aligned and joined with super glue, and the material properties will not change over time (as does the hydrogel in [16], [17]). Simulations verified that small fabrication differences (e.g., thin air gaps between plastic and ceramic layers) affect antenna performance by less than 15% across the bandwidth. Note that air is used as a worst-case scenario as its permittivity is lower than that anticipated by the glue (e.g., in [40] sprayable glue had a relative permittivity of 2).

The experimental setup is displayed in Fig. 5(b). The conductors of the HCLA are soldered to the Mini-Circuits balun, and the balun is connected to the network analyzer. Styrofoam is used to hold the balun in place. The antenna is placed on the SPEAG POPEYE-V10 [41] or ground beef (as in Fig. 5(b)) phantom depending on the requirements of the experiment. The former phantom is used for ease of measurement as it an accurate and reproducible material representative of the human body. The latter is a well-recognized phantom with similar electrical properties to biological tissues [42] and is used as a moldable material that can be adjusted experimentally to represent different tissue depths. For example, implant antennas can be fully surrounded by ground beef as they would be surrounded by tissues in the body. The properties of ground beef, however, may not be stable due to changes in temperature, fat content, and/or freshness.

V. Results

A. Reflection Coefficient

The simulated versus measured reflection coefficient of the HCLA is displayed in Fig. 7. The simulation setup of Fig. 5(a) was employed with the tissue box emulating the properties of the POPEYE phantom. Two identical HCLA antennas were fabricated using the process described in Section IV. The measurement setup is displayed in Fig. 5(b), where in this case the POPEYE phantom material is used instead of ground beef. As seen, the measured results are similar to the simulated results, Fig. 7, particularly in regard to the bandwidth. The reflection coefficient is below -10 dB across most of the 1 to 5 GHz frequency range. The measured low frequency cutoff is 1.38 GHz, and the measured high frequency cutoff is 4.95 GHz. From 2.5 to 3.6 GHz, the reflection coefficient rises above the targeted value of -10 dB; however, the reflection coefficient remains below -6 dB, which can be deemed acceptable. The first resonance is the dominant TM_{10} mode of the quasi-bowtie antenna, and the second resonance is a higher order mode [26]. Additionally, the measured results are shifted to a higher frequency than the simulation results. The abovementioned discrepancies from simulation can be attributed to the presence of the balun and the lack of glue layers in simulations.

Notably, the measured results of the two HCLAs, namely Antenna 1 and Antenna 2 in Fig. 7, are very similar. The low frequency cutoff demonstrates the greatest error between the antennas with an approximately 18% difference between Antenna 1 and Antenna 2; however, this error is similar to the expected error determined from simulations. The antennas match exceptionally well across the rest of the bandwidth, thus demonstrating that the fabrication process is repeatable. The antennas have consistent performance which is not significantly impacted by minor changes in the antenna that may occur (e.g., misalignment between ceramic and plastic layers, air or glue gaps). Performance also remained the same over the course of the two months that the antenna was measured.

B. Transmission Loss with Wireless Implants

The transmission loss of the HCLA was simulated and measured with a wireless implant antenna. The latter is a small patch antenna with dimensions of 11.5 mm by 18.5 mm, operating in the 2.4 GHz ISM band with 360 MHz bandwidth (see inset of Fig. 8). The antenna was placed 3 cm inside of the ground beef to represent a deep-tissue implant. The HCLA was then placed on top of the ground beef to act as the external antenna. Careful attention was made to ensure alignment between the implant and the HCLA. The simulated versus measured transmission coefficient is seen in Fig. 8. The

This article has been accepted for publication in IEEE Transactions on Antennas and Propagation. This is the author's version which has not been fully edited and content may change prior to final publication. Citation information: DOI 10.1109/TAP.2022.3188354

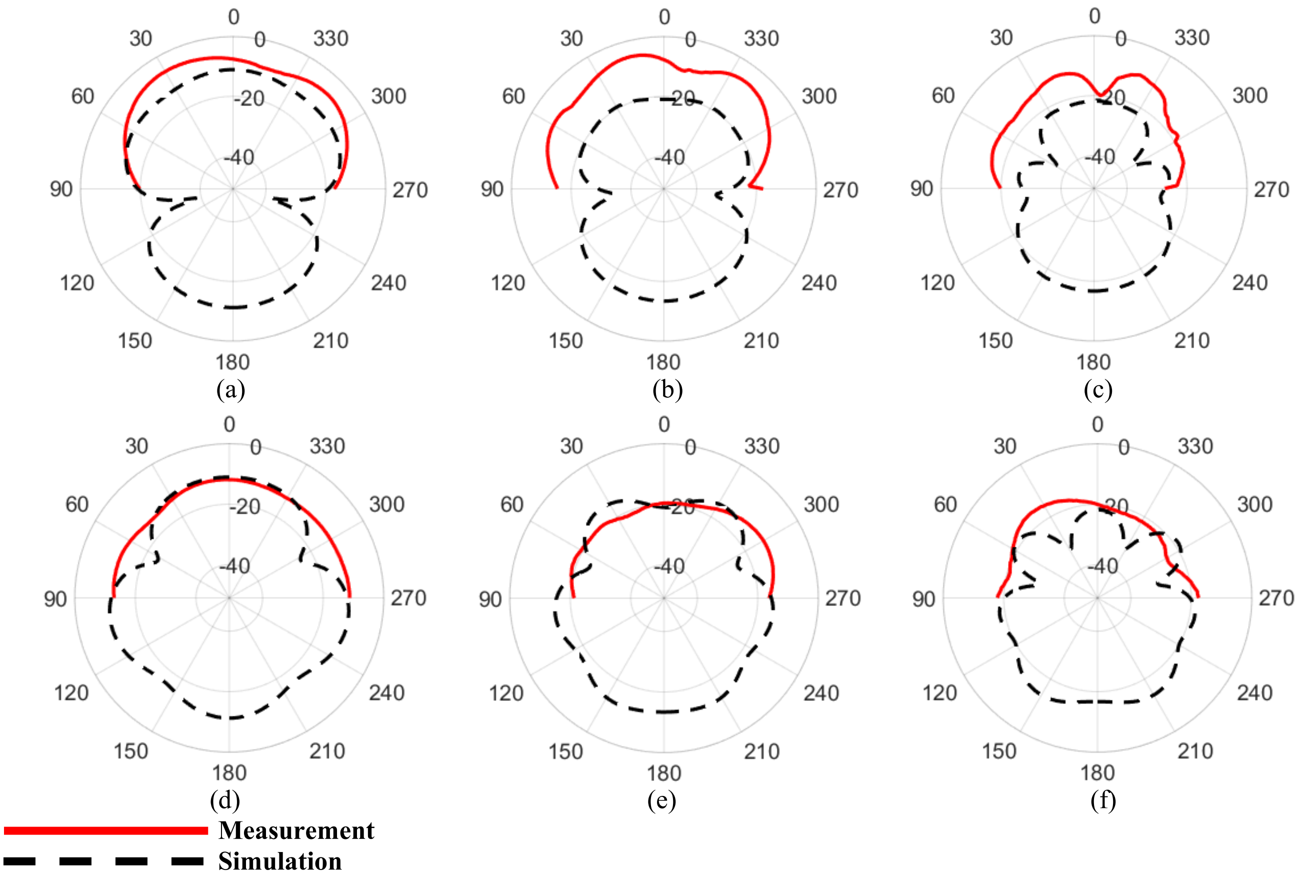

Fig. 11. Simulated versus measured radiation patterns of the (a)-(c) horizontal phantom orientation and (d)-(f) vertical phantom orientation and 2, 3, and 4 GHz, respectively.

transmission loss is 21.78 dB at 2.4 GHz, which is a 5.72 dB improvement over previous into-body antennas (Table I). The measured results closely match the simulated results. The transmission coefficient is maximum around 2.4 GHz, which is expected due to the properties of the implant.

C. Transmission Loss with Broadband Antennas

The transmission loss of the HCLA was also measured with a broadband antenna. A broadband antenna will allow for better characterization of the transmission across the full bandwidth, rather than focusing on a single frequency point, as with the implant antenna. A spiral antenna was selected, having a diameter of 14.5 cm, and exhibiting measured and simulated reflection below -10 dB across the entire frequency range (see inset in Fig. 9). A 3 cm layer of ground beef was placed on the spiral antenna, and the HCLA was placed on top of the ground beef, to emulate transmission between biological tissues. The HCLA was centered over the spiral antenna to ensure proper alignment and minimize losses. The simulated versus measured reflection coefficient is displayed in Fig. 9. As seen, the measured values closely match the simulated values. The transmission loss varies across the bandwidth with a minimum transmission loss of 18.32 dB at 1.65 GHz. Loss is expected to increase with frequency due to the penetration depth of electromagnetic waves into the biological tissues [25].

D. Radiation Patterns

The radiation patterns of the HCLA were measured in an anechoic chamber. The antenna is designed to radiate effectively into the biological tissues; however, it is not straightforward to experimentally retrieve simulated radiation patterns inside a solid (SPEAG POPEYE) or semi-solid (ground beef) phantom. However, some of the radiation escapes into the air instead of the tissues in the form of “back-lobe” radiation that can be measured in the anechoic chamber, Fig. 10.

Measurements of the back lobe patterns were performed in two planes. The first involved the POPEYE phantom oriented horizontally on the foam column, Fig. 10(a), and the second involved the POPEYE phantom oriented vertically on the foam column, Fig. 10(b). The radiation patterns were measured from 0.7 to 5 GHz in 5 MHz frequency intervals. Only the back lobe radiation patterns, from -90° to 90°, were measured. The results of the chamber measurements are seen in Fig. 11. Here, Fig. 11(a)-(c) illustrates the measured versus simulated pattern in the horizontal phantom orientation at 2, 3, and 4 GHz, respectively. Fig. 11(d)-(f) illustrates the measured versus simulated pattern in the vertical phantom orientation at 2, 3, and 4 GHz, respectively. The top half of each pattern plot represents the measured (red) and simulated (black) back lobes. The bottom half of each pattern plot represents the simulated radiation into the phantom.

In general, the measured and simulated results follow similar patterns and have similar magnitude, particularly at 2 GHz. These three frequency points of 2, 3, and 4 GHz were selected to provide a summary of performance within the operational band of the HCLA, but other frequencies display similar trends. Larger discrepancies appear between the measured at simulated

This article has been accepted for publication in IEEE Transactions on Antennas and Propagation. This is the author's version which has not been fully edited and content may change prior to final publication. Citation information: DOI 10.1109/TAP.2022.3188354

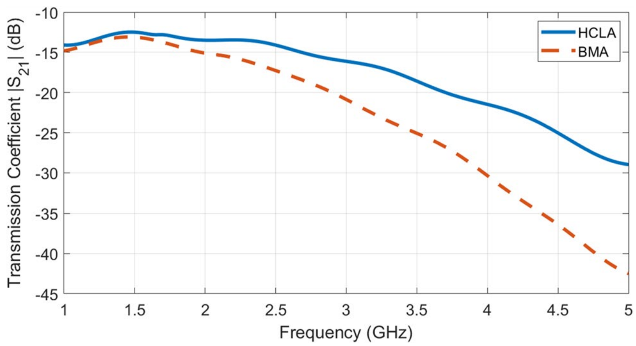

Fig. 12. Simulated transmission coefficient ($|S_{21}|$) of the HCLA versus the BMA between 3 cm of two thirds muscle phantom.

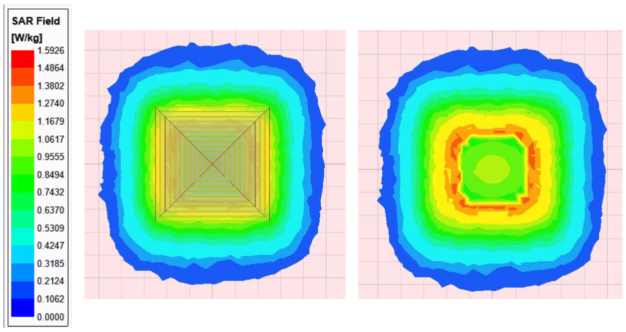

(a) (b)

Fig. 13. SAR_{1g} performance of the ceramic and plastic antenna at 2.4 GHz assuming an input power of 13.79 dBm illustrated (a) with and (b) without the antenna on the phantom

values at higher frequencies. There are several reasons why these differences may have occurred. First, the measurement setup in the chamber was very complex. The solid phantom created instability in the measurement because of its bulky size (177 mm width, 170 mm depth, 1000 mm height) and weight (13.5 Kg) [41]. Ensuring the antenna was both fully flush against the phantom and aligned at the correct angle was challenging. It was a significant effort to balance the phantom, balun, and antenna on the foam column such that none of the components moved as the column rotated during the measurements. The exact angles that were measured may not perfectly align with the simulated angles, further contributing to potential errors. Measuring additional planes or measuring the full 3D pattern could provide a more complete, accurate picture of the actual back lobe radiation. Additionally, the balun, while necessary for proper feeding, could have interfered with the radiation pattern measurements. Particularly in the horizontal orientation, Fig. 10(a), the balun, seen on the right covered in green tape, likely interfered with the radiation pattern because it was blocking the line-of-sight between the HCLA and the chamber measurement antenna. Given the good agreement of the measured back lobe patterns with the simulated ones, we can assume the simulated into-body patterns are a reasonable estimate of the radiation occurring inside the tissue. In the future, back lobe radiation can be minimized, if desired, by adding a ground plane or absorbing materials to the antenna.

E. Comparison to Bio-Matched Antennas

Multiple simulations were performed to verify the layered ceramic and plastic dielectric of the HCLA has improved performance compared to the previous BMA in [17], [18]. The simulation setup is shown in Fig 5(a). The HCLA or BMA respectively were placed on either side of the 3 cm tissue box emulating the properties of 2/3 muscle. Fig. 12 demonstrates the simulated transmission coefficient from 1 to 5 GHz of the two antennas. Clearly, the HCLA significantly outperforms the BMA in terms of transmission loss, especially at higher frequencies. At 4.8 GHz (a frequency used for implants in [23], [24] and for radiometry in [16]), the HCLA demonstrates ~12.5 dB improvement in transmission loss over the BMA.

F. Specific Absorption Rate

Specific Absorption Rate (SAR) simulations were performed for the HCLA using the simulation setup displayed in Fig. 5(a) with the tissue box emulating the properties of the POPEYE phantom. The Federal Communications Commission (FCC) guidelines state that the SAR limit is 1.6 W/kg, averaged over 1g of tissue [43]. The SAR guidelines are intended to limit human exposure to radio frequency energy for health and safety purposes. The 2.4 GHz SAR distribution over 1g of tissue is illustrated in Fig. 13. For an input power of 13.79 dBm, or 0.025 W, the maximum value of SAR_{1g} is approximately 1.6 W/kg. Input power levels as high as 13.79 dBm will meet the strictest safety standards set by the FCC.

VI. Conclusion

In this paper, we presented a high-contrast low-loss antenna (HCLA) capable of efficient transmission into biological tissues for medical telemetry, sensing, and imaging applications. The antenna operates across the 1 to 5 GHz bandwidth, and its key novelty is the use of low-loss materials with a 3D engineered dielectric to improve gain and directivity. The alternating layers of high and low permittivity materials convert the outgoing spherical waves into planar wavefronts, and the high permittivity material minimizes mismatch between the antenna-skin interface. The HCLA addresses previous limitations of into-body antennas by incorporating stable, low-loss and biocompatible materials with a repeatable fabrication process.

Both simulation and measurement results indicate that the HCLA demonstrates improved transmission into biological tissues across the bandwidth. The transmission loss to a wireless implant at 2.4 GHz is 21.78 dB, providing 5.72 dB improvement over previous technologies. The antenna also shows efficient transmission to a broadband antenna. The HCLA shows significant improvement over the BMA, with a 12.5 dB improvement in transmission loss at 4.8 GHz. The radiation patterns of the back lobe of the antenna were measured in an anechoic chamber. The measured patterns are similar to the simulated patterns, particularly at lower frequencies. The HCLA meets SAR standards set by the FCC for input power levels as high as 13.79 dBm, or 0.025 W.

The HCLA is a big step forward for into-body antennas with multiple improvements over current technologies. The antenna shows promise for potential integration into emerging medical device technologies. Future work will focus on modification of the balun to further improve transmission loss, minimizing back lobe radiation to reduce electromagnetic interference, wearable implementation via e-textiles or e-fabrics, and integrating the antenna into telemetry, sensing, and/or imaging applications.

VII. References

[1] C. W. L. Lee, A. Kiourti, J. Chae, and J. L. Volakis, "A High-Sensitivity Fully Passive Neurosensing System for Wireless Brain Signal Monitoring," *IEEE Trans. Microwave Theory Techn.*, vol. 63, no. 6, pp. 2060–2068, Jun. 2015, doi: 10.1109/TMTT.2015.2421491.

[2] Y. Liu, Y. Chen, H. Lin, and F. H. Juwono, "A Novel Differentially Fed Compact Dual-Band Implantable Antenna for Biotelemetry Applications," *IEEE Antennas and Wireless Propagation Letters*, vol. 15, pp. 1791–1794, 2016, doi: 10.1109/LAWP.2016.2536735.

[3] E. Y. Chow, Y. Ouyang, B. Beier, W. J. Chappell, and P. P. Irazoqui, "Evaluation of Cardiovascular Stents as Antennas for Implantable Wireless Applications," *IEEE Transactions on Microwave Theory and Techniques*, vol. 57, no. 10, pp. 2523–2532, Oct. 2009, doi: 10.1109/TMTT.2009.2029954.

[4] A. Kiourti, J. R. Costa, C. A. Fernandes, and K. S. Nikita, "A Broadband Implantable and a Dual-Band On-Body Repeater Antenna: Design and Transmission Performance," *IEEE Transactions on Antennas and Propagation*, vol. 62, no. 6, pp. 2899–2908, Jun. 2014, doi: 10.1109/TAP.2014.2310749.

[5] M. K. Magill, G. A. Conway, and W. G. Scanlon, "Tissue-Independent Implantable Antenna for In-Body Communications at 2.36–2.5 GHz," *IEEE Transactions on Antennas and Propagation*, vol. 65, no. 9, pp. 4406–4417, Sep. 2017, doi: 10.1109/TAP.2017.2708119.

[6] M. K. Magill, G. A. Conway, and W. G. Scanlon, "Circularly Polarized Dual-Mode Wearable Implant Repeater Antenna With Enhanced Into-Body Gain," *IEEE Transactions on Antennas and Propagation*, vol. 68, no. 5, pp. 3515–3524, May 2020, doi: 10.1109/TAP.2020.2972335.

[7] H. Bahrami, S. A. Mirbozorgi, R. Ameli, L. A. Rusch, and B. Gosselin, "Flexible, Polarization-Diverse UWB Antennas for Implantable Neural Recording Systems," *IEEE Transactions on Biomedical Circuits and Systems*, vol. 10, no. 1, pp. 38–48, Feb. 2016, doi: 10.1109/TBCAS.2015.2393878.

[8] L.-J. Xu, Z. Duan, Y.-M. Tang, and M. Zhang, "A Dual-Band On-Body Repeater Antenna for Body Sensor Network," *IEEE Antennas and Wireless Propagation Letters*, vol. 15, pp. 1649–1652, 2016, doi: 10.1109/LAWP.2016.2520023.

[9] J. M. Felício, J. R. Costa, and C. A. Fernandes, "Dual-Band Skin-Adhesive Repeater Antenna for Continuous Body Signals Monitoring," *IEEE Journal of Electromagnetics, RF and Microwaves in Medicine and Biology*, vol. 2, no. 1, pp. 25–32, Mar. 2018, doi: 10.1109/JERM.2018.2806186.

[10] D. B. Rodrigues *et al.*, "Design and Optimization of an Ultra Wideband and Compact Microwave Antenna for Radiometric Monitoring of Brain Temperature," *IEEE Trans. Biomed. Eng.*, vol. 61, no. 7, pp. 2154–2160, Jul. 2014, doi: 10.1109/TBME.2014.2317484.

[11] N.-A. Livanos *et al.*, "Design and Interdisciplinary Simulations of a Hand-Held Device for Internal-Body Temperature Sensing Using Microwave Radiometry," *IEEE Sensors J.*, vol. 18, no. 6, pp. 2421–2433, Mar. 2018, doi: 10.1109/JSEN.2018.2791443.

[12] P. Momenroodaki, W. Haines, M. Fromandi, and Z. Popovic, "Noninvasive Internal Body Temperature Tracking With Near-Field Microwave Radiometry," *IEEE Transactions on Microwave Theory and Techniques*, vol. 66, no. 5, pp. 2535–2545, May 2018, doi: 10.1109/TMTT.2017.2776952.

[13] T. Sugiura, H. Hirata, J. W. Hand, J. M. J. Van Leeuwen, and S. Mizushina, "Five-band microwave radiometer system for noninvasive brain temperature measurement in newborn babies: Phantom experiment and confidence interval," *Radio Science*, vol. 46, no. 5, 2011, doi: 10.1029/2011RS004736.

[14] A. E. Fouda and F. L. Teixeira, "Ultra-wideband microwave imaging of breast cancer tumors via Bayesian inverse scattering," *Journal of Applied Physics*, vol. 115, no. 6, p. 064701, Feb. 2014, doi: 10.1063/1.4865327.

[15] M. Klemm *et al.*, "Development and testing of a 60-element UWB conformal array for breast cancer imaging," in *Proceedings of the 5th European Conference on Antennas and Propagation (EUCAP)*, Apr. 2011, pp. 3077–3079.

[16] K. Tisdale, A. Bringer, and A. Kiourti, "Development of a Coherent Model for Radiometric Core Body Temperature Sensing," *IEEE Journal of Electromagnetics, RF and Microwaves in Medicine and Biology*, 2022.

[17] J. Blauert and A. Kiourti, "Bio-Matched Horn: A Novel 1–9 GHz On-Body Antenna for Low-Loss Biomedical Telemetry With Implants," *IEEE Transactions on Antennas and Propagation*, vol. 67, no. 8, pp. 5054–5062, Aug. 2019, doi: 10.1109/TAP.2018.2889159.

[18] J. Blauert and A. Kiourti, "Theoretical Modeling and Design Guidelines for a New Class of Wearable Bio-Matched Antennas," *IEEE Transactions on Antennas and Propagation*, vol. 68, no. 3, pp. 2040–2049, Mar. 2020, doi: 10.1109/TAP.2019.2948727.

[19] A. Andryieuski, S. M. Kuznetsova, S. V. Zhukovsky, Y. S. Kivshar, and A. V. Lavrinenko, "Water: Promising Opportunities For Tunable All-dielectric Electromagnetic Metamaterials," *Sci Rep*, vol. 5, p. 13535, Aug. 2015, doi: 10.1038/srep13535.

[20] A. Rice and Kiourti, Asimina, "Real World Considerations for Into-Body Antennas," presented at the IEEE International Symposium on Antennas and Propagation and USNC-URSI Radio Science Meeting, 2022.

[21] "Zirconia Oxide Ceramics ZrO2," *Ortech Advanced Ceramics*. https://www.ortechceramics.com/creamic-materials/zirconia-oxide/ (accessed Dec. 29, 2021).

[22] E. Huber, M. Mirzaee, J. Bjorgaard, M. Hoyack, S. Noghanian, and I. Chang, "Dielectric property measurement of PLA," in *2016 IEEE International Conference on Electro Information Technology (EIT)*, May 2016, pp. 0788–0792. doi: 10.1109/EIT.2016.7535340.

[23] W.-C. Chen, C. W. L. Lee, A. Kiourti, and J. L. Volakis, "A Multi-Channel Passive Brain Implant for Wireless Neuropotential Monitoring," *IEEE Journal of Electromagnetics, RF and Microwaves in Medicine and Biology*, vol. 2, no. 4, pp. 262–269, Dec. 2018, doi: 10.1109/JERM.2018.2877330.

[24] H. N. Schwerdt *et al.*, "A Fully Passive Wireless Microsystem for Recording of Neuropotentials Using RF Backscattering Methods," *Journal of Microelectromechanical Systems*, vol. 20, no. 5, pp. 1119–1130, Oct. 2011, doi: 10.1109/JMEMS.2011.2162487.

[25] D. Nikolayev, M. Zhadobov, P. Karban, and R. Sauleau, "Electromagnetic Radiation Efficiency of Body-Implanted Devices," *Phys. Rev. Applied*, vol. 9, no. 2, p. 024033, Feb. 2018, doi: 10.1103/PhysRevApplied.9.024033.

[26] C. A. Balanis, *Antenna theory: analysis and design*, Fourth edition. Hoboken, New Jersey: Wiley, 2016.

[27] H. Eskandari, T. Tyc, J. L. Albadalejo-Lijarcio, O. Zetterstrom, and O. Quevedo-Teruel, "Design of an Impedance-Matched Horn Antenna with Enhanced Directivity Using Conformal Transformation Optics," in *2020 14th European Conference on Antennas and Propagation (EuCAP)*, Copenhagen, Denmark, Mar. 2020, pp. 1–4. doi: 10.23919/EuCAP48036.2020.9135870.

[28] X. Chen and Y. Ge, "Enhancing the Radiation Performance of a Pyramidal Horn Antenna by Loading a Subwavelength Metasurface," *IEEE Access*, vol. 5, pp. 20164–20170, 2017, doi: 10.1109/ACCESS.2017.2755680.

[29] T. Ding, J. Yi, H. Li, H. Zhang, and S. N. Burokur, "3D field-shaping lens using all-dielectric gradient refractive index materials," *Sci Rep*, vol. 7, no. 1, p. 782, Dec. 2017, doi: 10.1038/s41598-017-00681-z.

[30] M. Q. Qi *et al.*, "Suppressing Side-Lobe Radiations of Horn Antenna by Loading Metamaterial Lens," *Sci Rep*, vol. 5, no. 1, p. 9113, Aug. 2015, doi: 10.1038/srep09113.

[31] Italian National Research Council Institute for Applied Physics, "Dielectric Properties of Body Tissues." http://niremf.ifac.cnr.it/tissprop/ (accessed Dec. 29, 2021).

[32] P. F. Manicone, P. Rossi Iommetti, and L. Raffaelli, "An overview of zirconia ceramics: Basic properties and clinical applications," *Journal of Dentistry*, vol. 35, no. 11, pp. 819–826, Nov. 2007, doi: 10.1016/j.jdent.2007.07.008.

[33] L. Yin, Y. Nakanishi, A.-R. Alao, X.-F. Song, J. Abduo, and Y. Zhang, "A Review of Engineered Zirconia Surfaces in Biomedical Applications," *Procedia CIRP*, vol. 65, pp. 284–290, 2017, doi: 10.1016/j.procir.2017.04.057.

[34] Y. Ramot, M. Haim-Zada, A. J. Domb, and A. Nyska, "Biocompatibility and safety of PLA and its copolymers," *Adv Drug Deliv Rev*, vol. 107, pp. 153–162, Dec. 2016, doi: 10.1016/j.addr.2016.03.012.

[35] C. for D. and R. Health, "Select Updates for Biocompatibility of Certain Devices in Contact with Intact Skin," *U.S. Food and Drug Administration*, Oct. 22, 2020. https://www.fda.gov/regulatory-information/search-fda-guidance-documents/select-updates-

biocompatibility-certain-devices-contact-intact-skin (accessed May 20, 2022).
[36] "Ceramic Substrates," *Ortech Advanced Ceramics*. https://www.ortechceramics.com/products/uncategorized/ceramic-substrates/ (accessed Dec. 29, 2021).
[37] "SCTX1-83-2W+," *Mini-Circuits*. https://www.minicircuits.com/WebStore/dashboard.html?model=SCTX1-83-2W%2B (accessed Dec. 29, 2021).
[38] "Resin Family: Rigid," *Formlabs*. https://formlabs.com/materials/rigid/ (accessed Dec. 29, 2021).
[39] "Form 2," *Formlabs*. https://formlabs.com/3d-printers/form-2/ (accessed Dec. 29, 2021).
[40] A. Kiourti, J. R. Costa, C. A. Fernandes, A. G. Santiago, and K. S. Nikita, "Miniature Implantable Antennas for Biomedical Telemetry: From Simulation to Realization," *IEEE Transactions on Biomedical Engineering*, vol. 59, no. 11, pp. 3140–3147, Nov. 2012, doi: 10.1109/TBME.2012.2202659.
[41] "POPEYE10 & mmW-POPEYE10," *SPEAG*. https://speag.swiss/products/em-phantoms/phantoms-3/ (accessed Dec. 29, 2021).
[42] K. Guido, C. Matos, J. Ramsey, and A. Kiourti, "Tissue-Emulating Phantoms for In Vitro Experimentation at Radio Frequencies: Exploring characteristics, fabrication, and testing methods," *IEEE Antennas and Propagation Magazine*, vol. 63, no. 6, pp. 29–39, Dec. 2021, doi: 10.1109/MAP.2020.3003208.
[43] "Wireless Devices and Health Concerns," *Federal Communications Commission*, May 26, 2011. https://www.fcc.gov/consumers/guides/wireless-devices-and-health-concerns (accessed Jan. 25, 2022).

Allyanna Rice (S'22) received the B.S. degree *(summa cum laude)* in electrical engineering from Clemson University, Clemson, SC, USA in 2020. She is currently pursuing the Ph.D. degree in electrical engineering with the ElectroScience Laboratory, The Ohio State University, Columbus, OH, USA, under the supervision of Dr. A. Kiourti.

From 2018 to 2021, she was an Intern with Johns Hopkins Applied Physics Laboratory, MIT Lincoln Laboratory, Herrick Technology Laboratories, and Viasat. Her current research interests include biomedical applications of electromagnetics, antennas, and wearable sensors.

Ms. Rice is a recipient of the 2021 NASA Space Technology Graduate Research Opportunities (NSTGRO) Award and was the recipient of the Ohio State College of Engineering Graduate Fellowship for 2020-2021. She is serving as a reviewer for IEEE Transactions on Antennas and Propagation

Asimina Kiourti (S'10, M'14, SM'19) received the Diploma degree in electrical and computer engineering from the University of Patras, Patras, Greece, in 2008, the M.Sc. degree in technologies for broadband communications from University College London, London, U.K., in 2009, and the Ph.D. degree in electrical and computer engineering from the National Technical University of Athens, Athens, Greece, in 2013.

She is currently an Assistant Professor of Electrical and Computer Engineering at The Ohio State University and the ElectroScience Laboratory, Columbus, OH, USA. From 2013 to 2016 she served as a Post-Doctoral Researcher and then a Senior Research Associate at the ElectroScience Laboratory. During her career, she has co-authored 1 book, 12 book chapters, 5 granted patents, over 65 journal papers, and over110 conference papers and abstracts. Her research interests include bio-electromagnetics, wearable and implantable antennas, sensors for body area applications, and functionalized e-textiles.

Dr. Kiourti has received several scholarly awards, including the 2021 NSF CAREER award, the 2021 40 Under 40 recognition by Columbus Business First, the 2018 URSI Young Scientist Award, the 2014 IEEE Engineering in Medicine and Biology Society (EMB-S) Young Investigator Award, the 2012 IEEE Microwave Theory and Techniques Society (MTT-S) Graduate Fellowship for Medical Applications, and the 2011 IEEE Antennas and Propagation Society (AP-S) Doctoral Research Award.

She is currently serving as the Senior Editor of the IEEE Open Journal of Antennas and Propagation, the Editor of the Bioelectromagnetics column of the IEEE Antennas and Propagation Magazine, and an Associate Editor for the IEEE Transactions on Antennas and Propagation, the IEEE Journal of Electromagnetics, RF and Microwaves in Medicine and Biology, and the IEEE Antennas and Propagation Magazine.